PROCEEDINGS, 47th Workshop on Geothermal Reservoir Engineering
Stanford University, Stanford, California, February 7-9, 2022
SGP-TR-223

Estimation of Statistical Properties of Fracture Networks from Thermal-tracer Experiments

Guofeng Song[1], Delphine Roubinet[2,*], Zitong Zhou[3], Xiaoguang Wang[4], Daniel M. Tartakovsky[3] and Xianzhi Song[1]

[1] State Key Laboratory of Petroleum Resources and Prospecting, China University of Petroleum, Beijing, Beijing 102249, China

[2] Geosciences Montpellier, CNRS-Montpellier University, France

[3] Department of Energy Resources Engineering, Stanford University, Stanford, CA 94305, USA

[4] College of Energy, Chengdu University of Technology, Chengdu, 610051, China

[*]Corresponding author: delphine.roubinet@umontpellier.fr

Keywords: Discrete Fracture Network, Properties estimates, Thermal-tracer experiments, Heat transport processes, Bayesian inference, Neural network surrogate models

ABSTRACT

A two-dimensional particle-based heat transfer model is used to train a deep neural network. The latter provides a highly efficient surrogate that can be used in standard inversion methods, such as grid search algorithms. The resulting inversion strategy is utilized to infer statistical properties of fracture networks (fracture density and fractal dimension) from synthetic thermal experimental data. The (to-be-estimated) fracture density is well constrained by this method, whereas the fractal dimension is harder to determine and requires adding prior information on the fracture network connectivity. The method is tested on several fracture networks and hydraulic conditions.

1. INTRODUCTION

Geothermal energy provides an attractive solution to global warming and the carbon crisis. Efficient exploitation of geothermal resources is the key to commercial and sustainable geothermal projects. As fractures represent the main flow and heat transfer pathways in geothermal reservoirs, they play a critical role in heat extraction performance. Hydraulic fracturing techniques are often required to supplement natural fractures with artificial ones in order to connect the injection and production wells. The operation scheme can be modified, and heat extraction lifetime can be prolonged, using the updated fracture information provided by thermal experiments. Therefore, it is of significant importance to collect fracture information before the system exploitation.

Various methods are used to collect and interpret information about a fracture network, including direct observations of outcrops, multi-scale geoelectrical measurements and hydraulic and tracer experiments in boreholes (Bonnet et al., 2001; Demirel et al., 2018; Dorn et al., 2012, 2013; Roubinet et al., 2018). The latter characterization methods provide data that are directly related to the hydrogeological properties controlling flow and transport in fractured systems. For example, pressure data collected in observation boreholes during hydraulic experiments has been used to characterize the system's heterogeneity (Lods et al, 2020). This information can be supplemented with chemical tracer experiments that characterize the fracture network and matrix block properties through the interpretation of breakthrough curves (Haddad et al., 2014; Roubinet et al., 2013). Heat tracers might provide similar information; they have recently been deployed to characterize various processes in the natural environment, e.g., to monitor groundwater in large-scale systems, quantify hydraulic exchanges between surface and subsurface, and study flow channeling at the fracture scale (Saar, 2011; Constantz, 2008; Bernardie et al., 2018). Heat experiments offer several advantages over chemical tracers. First, distributed temperature sensors can be deployed along wellbores. Second, heat transfer covers larger areas than solute diffusion. Third, they are largely free from environmental constraints.

As data collected during thermal experiments contain information about the fracture network properties (Roubinet et al., 2015), inversion of these data should help in characterizing fractured rock. However, large-scale systems with complex fracture configurations require sophisticated inversion strategies, which are usually limited to only a few fractures (Fischer et al., 2018; Ringel et al., 2019). This is in contradiction with statistical fracture network models that are used in geothermal studies; these require the knowledge of large-scale network properties such as fracture density and fractal dimension (Gisladottir et al., 2016) . Both parameters impact flow and transport in fractured systems, the former characterizing the quantity of fractures present in the system and the latter the complexity of the fracture length distribution (Gisladottir et al., 2016). Estimation of such parameters requires repeated computations of the forward model for a large number of combinations of the fracture density and fractal dimension values that should vary over a wide range. Since this task is seldom possible with physics-based models, we deploy a neural network surrogate to be able to perform millions of forward simulations within a reasonable computation budget.

Our recent work demonstrates the potential of this strategy (Zhou et al., 2021). We used a physics-based forward model to train a deep neural network (DNN) and then used that surrogate for ensemble-based computation to develop an inversion method. This enabled us to infer the statistical properties of a fracture network from cross-borehole thermal experiments (CBTEs). A two-dimensional particle-tracking method is employed to solve the physics-based model. The negligible computational cost of the surrogate facilitates the deployment of a greedy grid search in the parameter space spanned by fracture density C and fractal dimension D. The inversion is done

via Bayesian update. The inversion with DNN-based surrogate in our approach is four orders of magnitude faster than the equivalent inversion based on the physics-based model. The study of Zhou et al. (2021) suggests that fracture density is well constrained by data but fractal dimension is harder to determine. Incorporation of the prior information like fracture connectivity improves the confidence in the predictions of *C* and *D*.

This conclusion is based on a single hydraulic regime, which makes it hard to ascertain its generality and impact of the hydraulic conditions on inversion performance. Our goal is to analyze the impact of these conditions, which modify the flow velocities in the fracture networks and heat transfer in the entire system. As in our previous work, we deploy the following procedure. First, the two-dimensional particle tracking method is used to solve the flow and heat-transfer equations in Discrete Fracture Networks (DFNs) for different hydraulic conditions and fracture parameters. Second, these solutions are used to train the DNN-based surrogate models for the three velocity conditions. Third, the surrogate models are used to compute the posterior distribution of the parameters *C* and *D* for the three hydraulic configurations. Finally, we evaluate the value of various prior information types for improving the estimates of these posterior distributions and compare the results obtained under the various flow velocity regimes. Some conclusions and suggestions about improving inversion performance are presented in the last section.

2. METHODOLOGY

2.1 Description of the Forward Models

The CBTEs are simulated with the help of three forward models: (i) a model of fracture networks that defines the considered geological system, (ii) a physics-based model for simulating fluid flow and heat transfer in fractured geothermal reservoirs and (iii) a DNN surrogate model to accurately and quickly predict the relative changes in temperature in the observation borehole.

2.1.1 Model of Fracture Networks

DFNs are generated via the fractal WT **(**Watanabe and Takahashi, 1995**)** model, which postulates the following power-law relationship among fracture parameters:

$$N_r = Cr^{-D} \tag{1}$$

where N_r is the number of fractures, and r is the relative length normalized by the smallest fracture length r_0. The parameters C and D denote fracture density and fractal dimension, respectively. Fracture centers are randomly distributed over a 100×100 m^2 domain with the same aperture of 5×10^{-4} m. The fractures are arranged at two preferred angles, $\theta_1 = 25°$ and $\theta_2 = 145°$.

2.1.2 Model of Flow and Heat Transfer in fractured systems

Flow in the fracture networks is modeled by coupling Poiseuille solution for single-phase steady-state laminar flow in individual planar fractures and flow conservation at the fracture intersections (Gisladottir et al. 2016; Zhou et al., 2021). We assume that the rock matrix is impervious to fluid and that the fluid is incompressible. The flow velocity u in the fractures and the mass conservation in each fracture node are expressed as

$$u = -\frac{gb^2}{12\nu} J \qquad \sum ub = 0 \tag{2}$$

where b is fracture aperture (m), J is hydraulic head gradient, and ν is fluid's kinematic viscosity (m^2/s). Constant hydraulic heads are enforced in the injection and observation wells, and the top and bottom boundaries are subjected to no flow conditions.

Heat transfer in individual fractures satisfies the advection-dispersion equation (3) and heat transfer in the rock matrix satisfies the diffusion equation (4) reduced to one-dimensional transversal diffusion (Gisladottir et al. 2016)

$$\frac{\delta T^f}{\delta t} + u\frac{\delta T^f}{\delta t} = D_L^f \frac{\partial^2 T^f}{\partial x^2} + D_T^f \frac{\partial^2 T^f}{\partial z^2} \tag{3}$$

$$\frac{\delta T^m}{\delta t} + u\frac{\delta T^m}{\delta t} = D_L^m \frac{\partial^2 T^m}{\partial x^2} + D_T^m \frac{\partial^2 T^m}{\partial z^2} \tag{4}$$

where u is the flow velocity computed with equation (2), D_L^f and D_T^f are the longitudinal and transversal dispersion coefficients, respectively, D_L^m and D_T^m are the longitudinal and transversal diffusion coefficients, respectively, and the subscripts m and f denote matrix and fracture, respectively. Heat flux at the fracture-matrix interface is defined as

$$T^f = T^m, \quad \phi D_T^m \frac{\partial T^m}{\partial z} = D_T^f \frac{\partial T^f}{\partial z}, \quad |z| = \frac{b}{2}\ . \tag{5}$$

The equations are solved via a particle-tracking method, which is significantly faster than mesh-based standard methods **(**Roubinet et al., 2010**)**. The cumulative distribution functions (CDFs) of particle arrival times describe the changes in the relative temperature T^* observed at the observation borehole,

$$T^* = \frac{T_{\text{obv}} - T_{in}}{T_{inj} - T_{in}} \tag{6}$$

where T_{in} is the initial fluid temperature in the system, and T_{inj} and T_{obs} are the temperatures at the injection and observation positions, respectively.

2.1.3 Deep Neural Network Model

DNN is used to replace the particle-based model to compute the ensemble-based simulations required for numerical inversion. The surrogate model is defined by

$$f:(C,D)\to Q(p), \quad \text{ICDF}: Q(p) = F^{-1}(p) = \min\{x\in R: F(x)\ge p\}, p\in(0,1) \tag{7}$$

where *Q(p)* is the inverse CDF, namely ICDF. We deploy a fully connected neural network (FCNN),

$$\begin{aligned} &\mathbf{NN}: \mathbf{m} \xrightarrow{FCNN} \hat{\mathbf{d}} \\ &\hat{\mathbf{d}} = \mathbf{NN}(\mathbf{m};\Theta) = (\sigma \circ \mathbf{W})(\mathbf{m}) \\ &\Theta = \arg\min_{\Theta} \sum_{i=1}^{N_{data}} \mathbf{\Lambda}(\mathbf{d_i}, \hat{\mathbf{d}}_i) \end{aligned} \tag{8}$$

where $\mathbf{m}$ denotes the parameters to be estimated, i.e., *C* and *D*. The vector $\mathbf{d}$ comprises the output of the physics-based model; $\hat{\mathbf{d}}$ contains the discretized values of the iCDF computed with the model **NN**; and Θ denotes weights of neurons, which can be obtained by minimizing the loss function $\mathbf{\Lambda}(\mathbf{d_i},\hat{\mathbf{d}}_\mathbf{i})$ between $\mathbf{d_i}$ and $\hat{\mathbf{d}}_\mathbf{i}$. We quantify the distance between two discrete distributions $P=(p_1,...,p_{N_k})$ and $P'=(p_1',...,p_{N_k}')$ in terms of the Hellinger distance (Le Cam, 2012),

$$\mathbf{\Lambda}(\mathbf{P},\mathbf{P}') = \frac{1}{\sqrt{2}}\left\|\sqrt{P}-\sqrt{P'}\right\|_2 = \left(\frac{1}{2}\sum_{i=1}^{N_k}\left(\sqrt{p_i}-\sqrt{p_i'}\right)^2\right)^{1/2}. \tag{9}$$

2.2 Description of the Inversion Model

Inversion via Bayesian update is adopted to obtain posterior probability density function (PDF) $f_{\mathbf{m}|\mathbf{d}}$ of the parameter vector $\mathbf{m}$. It is expressed by

$$f_{\mathbf{m}|\mathbf{d}}(\tilde{\mathbf{m}};\tilde{\mathbf{d}}) = \frac{f_{\mathbf{m}}(\tilde{\mathbf{m}})\, f_{\mathbf{d}|\mathbf{m}}(\tilde{\mathbf{m}};\tilde{\mathbf{d}})}{f_{\mathbf{d}}(\tilde{\mathbf{d}})}, \quad f_{\mathbf{d}}(\tilde{\mathbf{d}}) = \int f_{\mathbf{m}}(\tilde{\mathbf{m}})\, f_{\mathbf{d}|\mathbf{m}}(\tilde{\mathbf{m}};\tilde{\mathbf{d}})\, d\tilde{\mathbf{m}} \tag{10}$$

where $\tilde{\mathbf{d}}$ and $\tilde{\mathbf{m}}$ are the deterministic outcomes of random variables $\mathbf{d}$ and $\mathbf{m}$, respectively; f_m is the prior PDF of $\mathbf{m}$; $f_{\mathbf{d}|\mathbf{m}}$ is the likelihood function; the normalizing factor $f_\mathbf{d}$ ensures that $f_{\mathbf{m}|\mathbf{d}}$ integrates to 1. The likelihood function has the form

$$f_{\mathbf{d}|\mathbf{m}}(\tilde{\mathbf{m}};\tilde{\mathbf{d}}) = \frac{1}{\sigma_d\sqrt{2\pi}}\exp\left[-\frac{1}{2}\frac{L_H(\tilde{\mathbf{d}}, g(\tilde{\mathbf{m}}))}{\sigma_d^2}\right]. \tag{11}$$

This PDF has the standard deviation σ_d (0.4 in this work) and is centered on the square root of the Hellinger distance between the data $\tilde{\mathbf{d}}$ predicted by the likelihood and the data $g(\tilde{\mathbf{m}})$ provided by the forward model. Additionally, prior information of $\tilde{\mathbf{m}}$ to the likelihood function is considered with the expression

$$f_{\mathbf{m}|\mathbf{d}}(\tilde{\mathbf{m}};\tilde{\mathbf{d}}) \propto = f_{\mathbf{d}|\mathbf{m}}(\tilde{\mathbf{m}};\tilde{\mathbf{d}})\left(f_{\mathbf{m}}(\tilde{\mathbf{m}})\right)^{\gamma} \tag{12}$$

where γ is the impact of the prior information. Two kinds of prior information are considered in this work: one is the correlation between *C* and *D* based on field data (Bonnet et al., 2001), the other is based on fracture connectivity defined by

$$f_{\mathbf{m}}(\tilde{\mathbf{m}}) \propto N_{con}^2(\tilde{\mathbf{m}}), \quad N_{con}\in[0,1,...,20], \tag{13}$$

where N_{con} is the number of connected fracture networks among 20 random realizations of a DFN characterized by each (*C*, *D*).

3. RESULTS

The impact of hydraulic conditions on the estimation of fracture network properties is studied by considering the fracture network models used in Gisladottir et al. (2016) and Zhou et al. (2021). The fracture networks are generated with the fractal model of Watanabe and Takahashi (1995), for which we want to infer the fracture network properties C and D that correspond to the fracture density and fractal dimension, respectively. The other fracture network properties, as well as the simulation parameters, are the same as in Gisladottir et al. (2016) and Zhou et al. (2021). The hydraulic condition considered in these studies, which corresponds to the hydraulic gradient $J = 0.01$, is defined here as the reference hydraulic condition leading to the reference flow velocity configuration. Lower or higher flow velocities are defined in the present study by decreasing or increasing the reference hydraulic gradient by one order of magnitude, i.e., by setting $J = 0.001$ or 0.1, respectively.

For each velocity configuration, the 2D particle tracking model presented in Section 2 is utilized to simulate synthetic data that are representative of the data collected during cross-borehole thermal experiments (CBTEs). We consider 10^4 pairs of the parameters C and D discretized over the ranges of values [2.5,6.5] and [1.0,1.3], respectively, and 20 simulations of fracture networks in order to account for the randomness of fractured systems. We compute the temperature in an observation borehole for different temperatures in the injection borehole; the results are reported as cumulative distribution functions (CDFs) that are averaged over the 20 simulations. Table 1 shows examples of these CDFs for 6 pairs of the parameters C and D and the three different velocity configurations. We also show the corresponding iCDFs, which are used in the surrogate models. We observe that increasing C results in faster thermal breakthrough curves, i.e., earlier arrival times, because increasing the fracture density leads to reducing the size of the matrix block distribution and, thus, the long times spent in the matrix domain. For similar values of C, we also observe that increasing D has the same impact because it increases the complexity of the fracture network organization and, as before, reduces the size of the matrix blocks. These results have the following implications for flow velocity. First, larger flow velocity in the system decreases the time over which the changes in temperature are observed because heat transfers quicker from the injection to the observation borehole. Second, low flow velocity in the system results in CDFs that are distinct from each other whereas the curves almost overlap for the high velocity configuration. This is due to the impact of flow velocity in the fractures on heat transfer between fracture and matrix. For high velocities, heat transfer in the matrix is limited to a small zone around the fractures and is very often not impacted by the size of the matrix blocks or the presence of the neighboring fractures. For low velocities, heat diffuses in deeper parts of the matrix domain, often reaching the neighboring fractures, and thus being impacted by the fracture network organization and matrix block size distribution. In other words, under low flow velocity conditions the temperature curves are more sensitive to the fracture network properties, implying that it might be easier to infer these properties from thermal data.

Table 1: Examples of CDFs and ICDFs for three different flow velocities.

	Low velocity configuration	Reference velocity configuration	High velocity configuration
CDFs	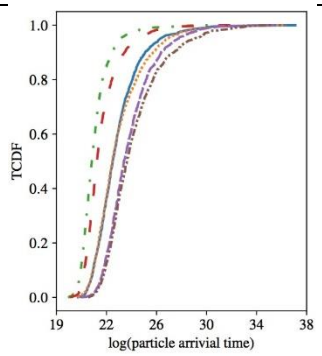	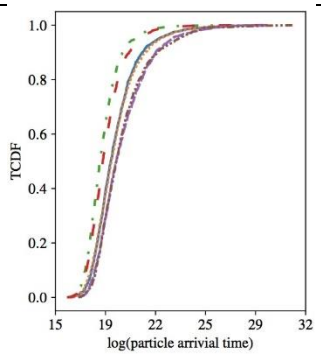	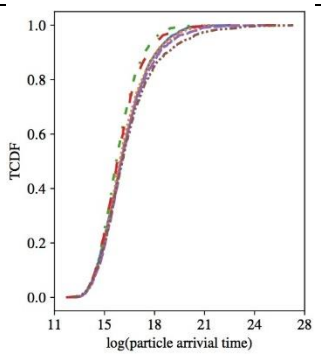
ICDFs	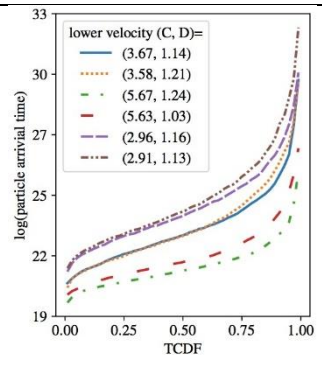	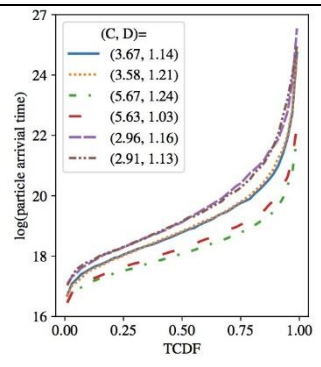	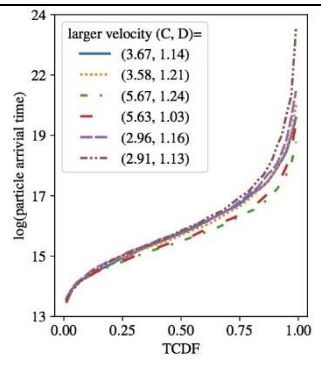

To verify whether decreasing flow velocity in the system helps one to infer the fracture network properties from thermal synthetic data, we build NN models as described in Section 2. For the three hydraulic configurations considered, the NN models are trained from the results obtained with the physics-based particle tracking simulations. The training loss of three resulting surrogate models is 0.079, 0.075

and 0.074, respectively. Figures 1 and 2 demonstrate the good fit between the predicted and reference data for 8 pairs of the parameters *C* and *D* for the low and high flow velocity configurations, respectively. This shows that our surrogate models are reliable to predict the changes in temperature for a large range of values of fracture network properties and hydraulic conditions.

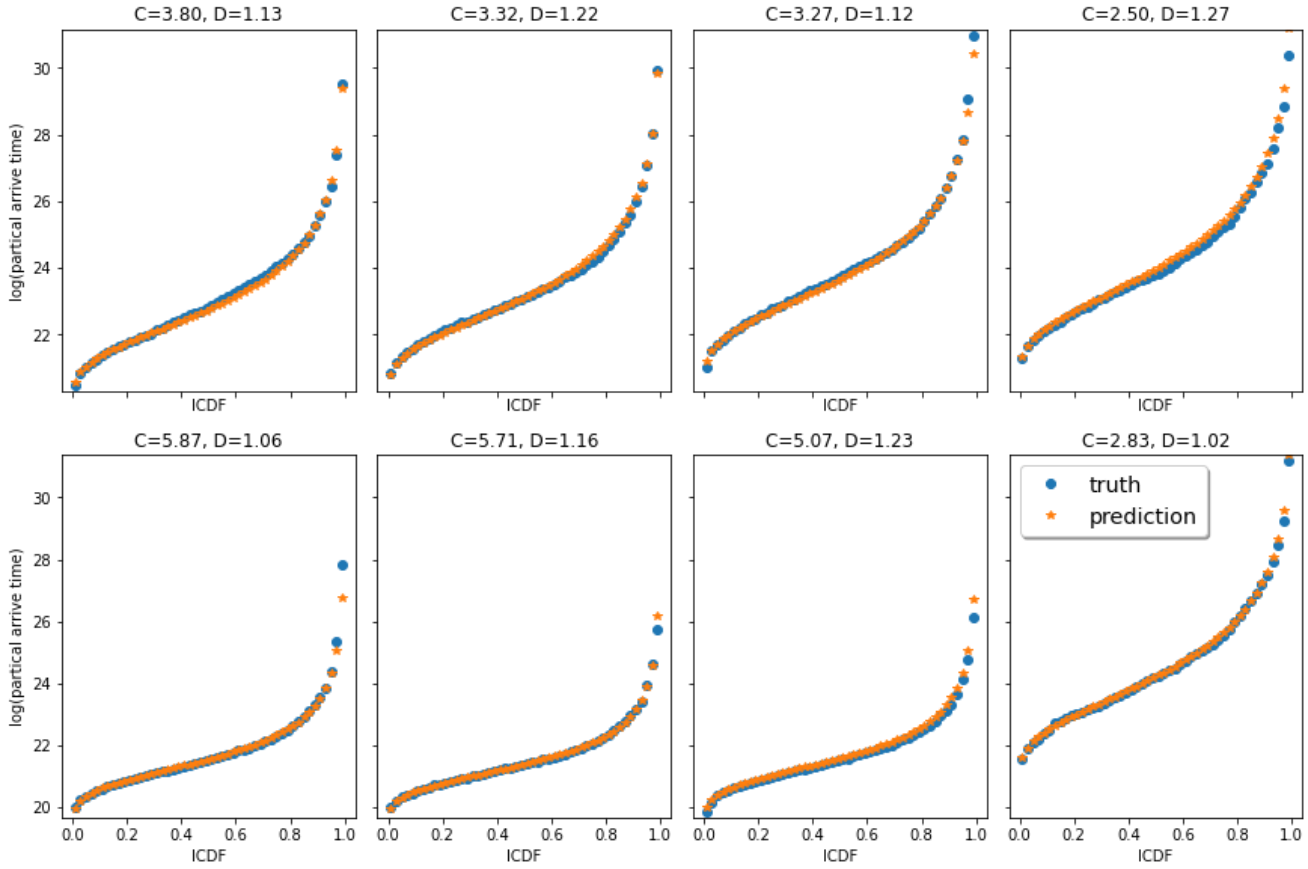

Figure 1: Examples of prediction of surrogate model for the low flow velocity configuration.

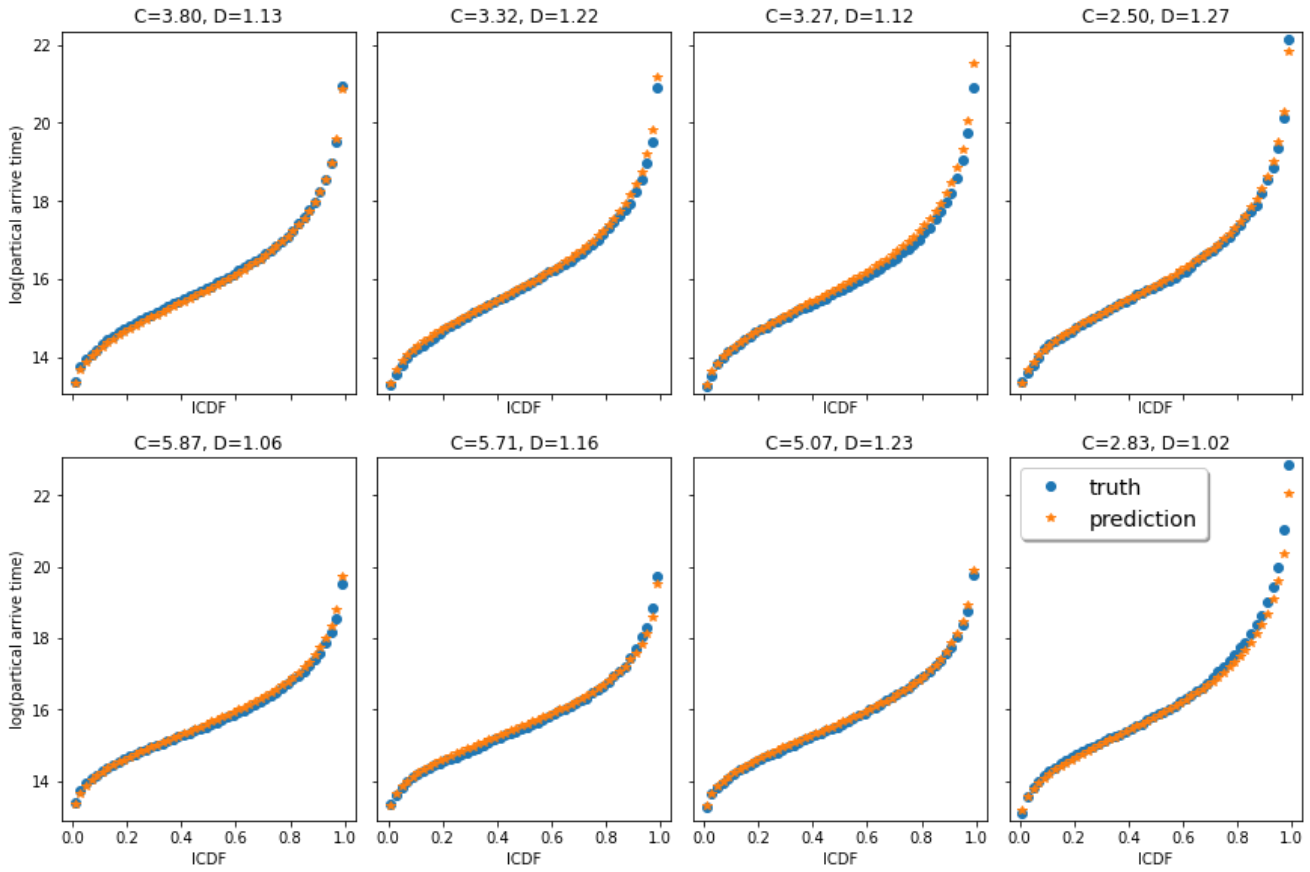

Figure 2: Examples of prediction of surrogate model for the high flow velocity configuration.

Our NN models enable us to conduct a large number of heat transfer simulations in complex fracture networks with reasonable computational times. They facilitate a detailed description of the posterior PDFs of parameters *C* and *D*, which are needed for Bayesian estimation of the unknown parameters from simple grid search algorithms. Table 2 shows examples of the posterior PDFs of *C* and *D* defined with 10^7 simulations. This high number of simulations is required to obtain well-defined PDFs and could not be done with (even the most efficient) physics-based models. The posterior PDFs of *C* and *D* are computed for the three hydraulic conditions mentioned before and considering various information. The results are provided without considering prior information (first row in Table 2) and with two kinds of prior information (prior1 and prior2) and two values of the parameter γ that defines the importance given to this prior information as described in Section 2. Prior1 (second and third rows in Table 2) corresponds to a correlation between the parameters *C* and *D* and deduced from field data, while prior2 (fourth and fifth row in Table 2) corresponds to a correlation in terms of connectivity of the fracture networks. All the details about this prior information and how they are integrated into the resulting posterior PDFs are provided in Zhou et al. (2021). In Table 2, the posterior PDFs are shown by considering the reference value (3.3602, 1.177075) for the parameter pair (*C*, *D*), which is represented as a blue circle on each figure.

From the results presented in Table 2, we observe that the posterior PDFs computed without prior information are well defined in the sense that the reference value is located in the highest probability zone that is represented in black and dark red. When increasing the flow velocity from the low to high velocity configurations, we observe that the extent of the highest probability zone increases in the horizontal direction and decreases in the vertical direction, suggesting that parameters C and D are easier to estimate from low and high velocity configurations, respectively. When adding prior information prior1 and prior2 with the parameter γ set to 0.5, the reference value is located in zones of high probability (red zones) but not in the highest probability zone that is represented in dark red. Increasing the value γ from 0.5 to 1 results in locating the reference value in zones of smaller probability, especially in the case of high velocity configuration for which the reference value is located in green to yellow zones. This demonstrates that, for the considered reference values, adding information on the correlation between parameters *C* and *D* that comes from field data and connectivity does not help to define the posterior PDFs of these parameters, and that this phenomenon is enhanced by increasing the importance of this information in the posterior PDFs definition.

Table 2: Examples of posterior PDFs of parameters *C* and *D* for three flow velocity.

	Low velocity configuration	Reference velocity configuration	High velocity configuration

Without prior, γ=0	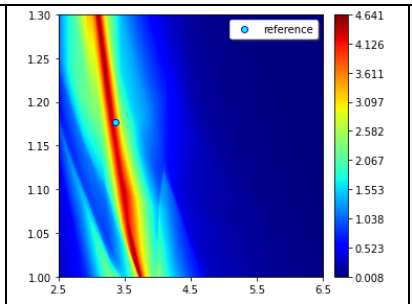	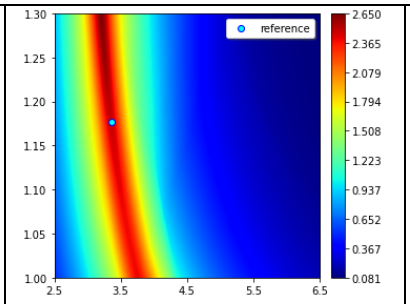	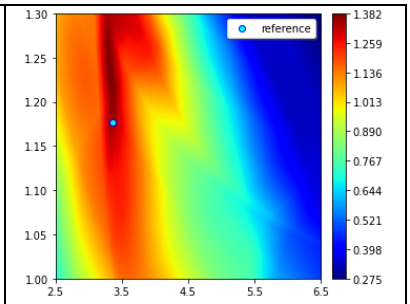
With prior1, γ=0.5	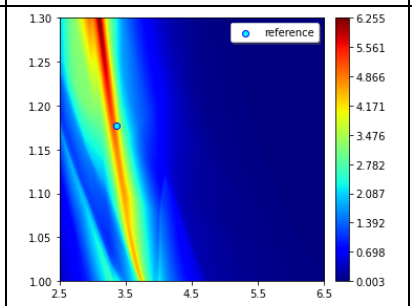	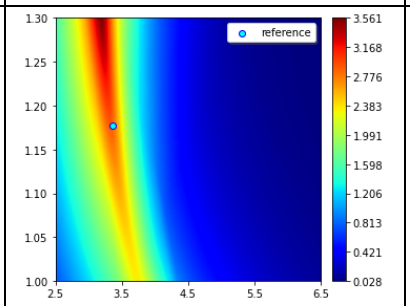	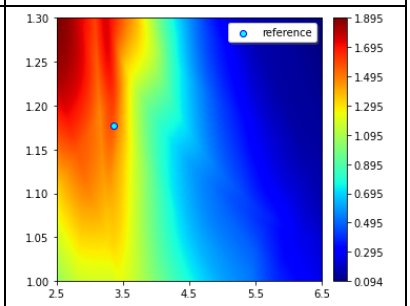
With prior1, γ=1	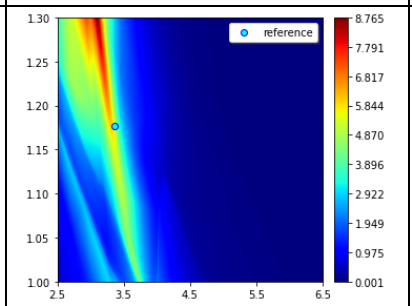	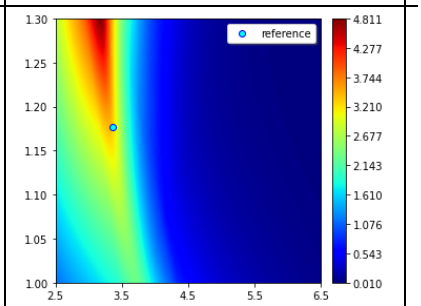	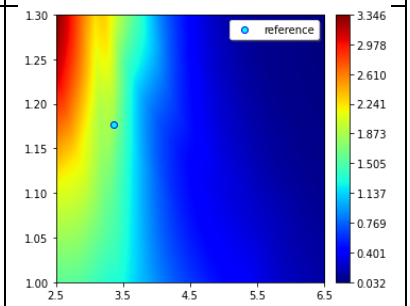
With prior2, γ=0.5	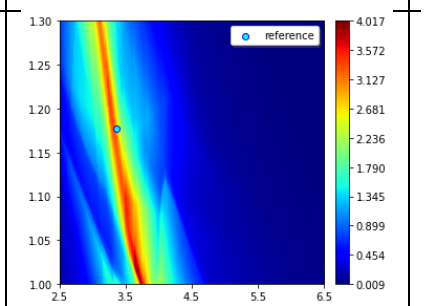	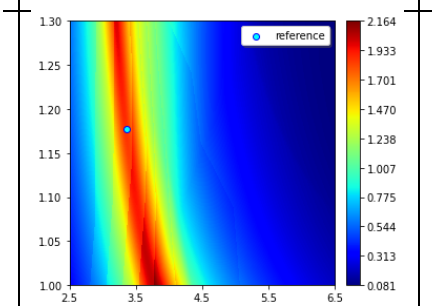	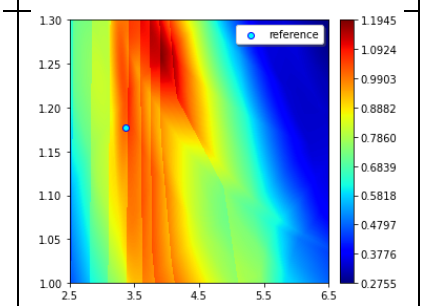
With prior2, γ=1	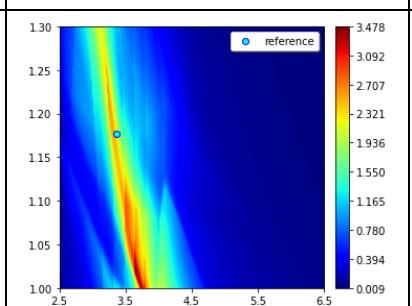	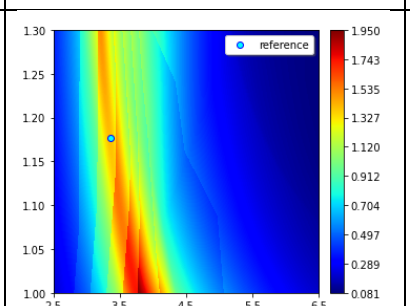	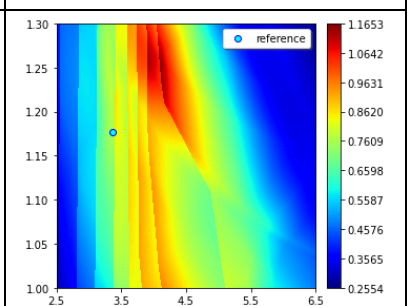

4. CONCLUSIONS AND DISCUSSION

We analyzed the impact of hydraulic conditions on the inversion performance of fracture network properties. The neural network surrogate models were built for three flow velocities to accurately predict the changes in relative temperature in an observation borehole. Fracture

density and fractal dimension were evaluated under different flow velocities and prior information. Our analysis leads to the following major conclusions.

1. Different surrogate models are obtained by DNN methods for three hydraulic configurations with a training loss of 0.079, 0.075 and 0.074, respectively. These surrogate models provide reliable predictions of the thermal breakthrough curves.

2. Fracture inversion performance of fracture network properties is improved under the lower and larger flow velocities. For the example that we studied, C is easier to estimate in the case of lower velocity because heat diffuses in deeper regions of the matrix, reaching the neighboring fractures, and thus being impacted by the fracture network organization and matrix block size distribution. On the other hand, it seems that D is more accurately inversed in the case of larger velocity, for which the fracture network complexity impacts thermal breakthrough curves. Therefore, suitable selection of velocity depends on the inversion interest.

3. With the reference values of C and D considered in this paper, adding information on the correlation from field data and fracture connectivity does not help to define the posterior PDFs of fracture density and fractal dimension. This phenomenon is enhanced by increasing the importance of this information in the posterior PDFs definition. Several more reference points should be included in future studies to evaluate the role of these priors.

There are some necessary modifications in future work. When working with new parameter values (other than C and D), the NN surrogates need to be trained again. This training could be speed up in future work with the use of *Transfer Learning*. Furthermore, the present study is conducted on 2D fracture networks to estimate two DFN parameters. The method is equally applicable to complicated 3D problems with more DFN characteristics, which may be the focus in future work. More specific evaluation of reference values should be defined to quantify the inversion performance of the proposed procedure. In addition, more types of prior information on C and D should be introduced to see if the inversion accuracy can be enhanced.

REFERENCES

Bonnet, E., Bour, O., Odling, N. E., Davy, P., Main, I., Cowie, P., & Berkowitz, B. (2001). Scaling of fracture systems in geological media. Reviews of Geophysics, 39(3), 347–383. https://doi.org/10.1029/1999RG000074

Constantz, J. (2008). Heat as a tracer to determine streambed water exchanges. Water Resources Research, 44, W00D10. https://doi.org/10.1029/2008WR006996

de La Bernardie, J., Bour, O., Le Borgne, T., Guihéneuf, N., Chatton, E., Labasque, T., & Gerard, M.-F. (2018). Thermal attenuation and lag time in fractured rock: Theory and field measurements from joint heat and solute tracer tests. Water Resources Research, 54, 10053–10075. https://doi.org/10.1029/2018WR023199

Demirel, S., Roubinet, D., Irving, J., & Voytek, E. (2018). Characterizing near-surface fractured-rock aquifers: Insights provided by the numerical analysis of electrical resistivity experiments. Water, 10(9), 1117. https://doi.org/10.3390/w10091117

Dorn, C., Linde, N., Le Borgne, T., Bour, O., & de Dreuzy, J.-R. (2013). Conditioning of stochastic 3-D fracture networks to hydrological and geophysical data. Advances in Water Resources, 62, 79–89. Part A(0). https://doi.org/10.1016/j.advwatres.2013.10.005

Fischer, P., Jardani, A., & Lecoq, N. (2018). Hydraulic tomography of discrete networks of conduits and fractures in a karstic aquifer by using a deterministic inversion algorithm. Advances in Water Resources, 112, 83–94. https://doi.org/10.1016/j.advwatres.2017.11.029

Gisladottir, V. R., Roubinet, D., & Tartakovsky, D. M. (2016). Particle methods for heat transfer in fractured media. Transport in Porous Media, 115(2), 311–326. https://doi.org/10.1007/s11242-016-0755-2

Haddad, A. S., Hassanzadeh, H., Abedi, J., & Chen, Z. (2014). Application of tracer injection tests to characterize rock matrix block size distribution and dispersivity in fractured aquifers. Journal of Hydrology, 510, 504–512. https://doi.org/10.1016/j.jhydrol.2014.01.008

Lods, G., Roubinet, D., Matter, J. M., Leprovost, R., Gouze, P., & Team, O. D. P. S. (2020). Groundwater flow characterization of an ophiolitic hard-rock aquifer from cross-borehole multi-level hydraulic experiments. Journal of Hydrology, 589, 125152. https://doi.org/10.1016/j.jhydrol.2020.125152

Ringel, L. M., Somogyvári, M., Jalali, M., & Bayer, P. (2019). Comparison of hydraulic and tracer tomography for discrete fracture network inversion. Geosciences, 9(6), 274. https://doi.org/10.3390/geosciences9060274

Roubinet, D., H.-H. Liu and J.-R. de Dreuzy (2010), A new particle-tracking approach to simulating transport in heterogeneous fractured porous media, Water Resources Research, 46, W11507, doi:10.1029/2010WR009371

Roubinet, D., De Dreuzy, J.-R., & Tartakovsky, D. M. (2013). Particle-tracking simulations of anomalous transport in hierarchically fractured rocks. Computers & Geosciences, 50, 52–58. https://doi.org/10.1016/j.cageo.2012.07.032

Roubinet, D., Irving, J., & Day-Lewis, F. D. (2015). Development of a new semi-analytical model for cross-borehole flow experiments in fractured media. Advances in Water Resources, 76, 97–108. https://doi.org/10.1016/j.advwatres.2014.12.002

Roubinet, D., Irving, J., & Pezard, P. A. (2018). Relating topological and electrical properties of fractured porous media: Insights into the characterization of rock fracturing. Minerals, 8(1), 14. https://doi.org/10.3390/min8010014

Saar, M. (2011). Review: Geothermal heat as a tracer of large-scale groundwater flow and as a means to determine permeability fields. Hydrogeology Journal, 19(1), 31–52. https://doi.org/10.1007/s10040-010-0657-2

Watanabe, K., & Takahashi, H. (1995). Fractal geometry characterization of geothermal reservoir fracture networks. Journal of Geophysical Research, 100(B1), 521–528. https://doi.org/10.1029/94JB02167

Zhou, Z., Roubinet, D., and Tartakovsky, D. M.: Thermal experiments for fractured rock characterization: theoretical analysis and inverse modeling, Water Resources Research, 57, e2021WR030608, (2021), doi:10.1029/2021WR030608

Zimmerman, R. A., & Tartakovsky, D. M. (2020). Solute dispersion in bifurcating networks. Journal of Fluid Mechanics, 901, A24. https://doi.org/10.1017/jfm.2020.573